Yield-aware Multi-Objective Optimization of a MEMS Accelerometer System Using QMC-Based Methodologies

Murat PAK[1.], Francisco V. FERNANDEZ[2.], Gunhan DUNDAR[1.]
[1.] Department of Electrical and Electronics Engineering, Bogazici University, Istanbul, Turkey.
E-Mails: murat.pak@boun.edu.tr, dundar@boun.edu.tr
[2.] IMSE, CSIC and University of Sevilla, Spain.
E-Mail: pacov@imse-cnm.csic.es

Abstract – This paper proposes a novel yield-aware optimization methodology that can be used for mixed-domain synthesis of robust micro-electro-mechanical systems (MEMS). The robust Pareto front optimization of a MEMS accelerometer system, which includes a capacitive MEMS sensor and an analog read-out circuitry, is realized by co-optimization of the mixed-domain system where the sensor performances are evaluated using highly accurate analytical models and the circuit level simulations are carried out by an electrical simulator. Two different approaches for yield-aware optimization have been implemented in the synthesis loop. The Quasi Monte Carlo (QMC) technique has been used to embed the variation effects into the optimization loop. The results for both two- and three-dimensional yield-aware optimization are quite promising for robust MEMS accelerometer synthesis.

I .INTRODUCTION

Due to physical heterogeneity, the design of MEMS, where the mechanical sensor and the electrical circuitry are co-designed, is a complex process where trial and error approaches are still widely used. This implies long design times and increased cost, which can be overcome by implementing automated optimization-based design methodologies. Besides shortening the design times and enabling optimal designs, these methodologies can also be used to enhance the yield of the synthesized designs.

Process variations play an important role in the robustness of mixed-domain MEMS and should be taken into account to avoid re-spins in the fabrication. In this paper, the yield-aware design of a MEMS accelerometer system is obtained by the co-optimization of the MEMS sensor and the read-out circuitry. For analog circuitry, it is a well-known fact that process variations have deteriorated along with the feature sizes scaling down; hence, the random physical variations originating from the manufacturing process have a much bigger impact on yield. The device geometry for the sensor is relatively large; however, even small variations on certain device parameters, such as the capacitive gap between the accelerometer electrodes, have a huge impact on the device performance. For that reason, considering these variations during the design process has become a must in order to guarantee robust system designs.

For the synthesis of MEMS sensors, several optimization-based approaches have been developed. In some of them, the sensor performances are evaluated by using special purpose MEMS simulators [1, 2] which are dedicated to MEMS design and modeling, while in others, accurate analytical models are used to speed up the optimization process [3, 4, 5].

Multi-domain optimization of the MEMS has also been reported [6, 7, 8]. In [6], mixed-domain circuit simulations are used to obtain the system performance for the MEMS. However, the synthesis only focuses on the MEMS sensor instead of the overall system. In the approach in [7], the sensor and the circuit are jointly simulated using behavioral models for system level design. Hence, the co-optimization for the MEMS is done using a high-level architectural description, rather than using device-level design parameters. A top-down methodology which is based on optimizing the sensor first and then the circuitry is developed in [8]. This type of methodology has several drawbacks, such as non-optimal partitioning of the specifications between sensor and circuitry, that cause suboptimal system designs [9].

In [8-9], even though the co-optimization of the mixed-domain MEMS has been carried out, process variations have not been taken into account. The mixed-domain MEMS co-optimization together with yield optimization has been addressed in [10]. A VerilogA circuit-level model of the capacitive MEMS accelerometer is used to enable fast evaluation and ease integration into the electrical simulator. This work starts from an initial nominal design and tunes this design for its yield optimization. For that, it makes use of yield analysis and the worst-case distance method, especially suited for high-yield values and a small number of parameters.

This paper presents a novel multi-objective yield-aware optimization methodology that realizes the co-optimization of the MEMS sensor and the read-out circuitry for both optimal and robust mixed-domain system performance. Unlike the approach in [10], it is not intended for yield optimization of an initial design, but for global design of hundreds of robust solutions, exhibiting the best trade-offs between different performances and with a reduced impact of process variations. The feasibility of the proposed approach is demonstrated by two- and three-dimensional optimizations of a capacitive MEMS accelerometer system.

The paper is organized as follows. Section 2 introduces the MEMS to be optimized, reviews different techniques for mixed-domain optimization as well as the yield-aware optimization and proposes the approach followed for the robust synthesis of the capacitive MEMS accelerometer. Section 3 describes the selection

of the optimization parameters, design variables and the objectives to be optimized. Section 4 shows the results for two- and three-dimensional yield-aware optimization of the MEMS accelerometer. Finally, Section 5 concludes the paper.

II. PROPOSED MULTI-OBJECTIVE YIELD-AWARE OPTIMIZATION TECHNIQUE FOR THE MEMS ACCELEROMETER SYSTEM

The accelerometer system used for the demonstration of the mixed-domain yield-aware optimization includes a capacitive sensor which was analytically modeled in [4] and a read-out circuitry based on a transimpedance amplifier [10]. Due to the different domains in the system, the MEMS sensor performance evaluations and the electrical simulations of the read-out circuitry are carried out separately. Optimizing the sensor and the circuit separately creates problems related to the composition of these individually optimized modules [9]. Moreover, the partitioning of the specifications (e.g., the partitioning of the system noise constraint which is contributed by the sensor and the amplifier during separate optimizations) is another problem. To address all these problems, a methodology based on the co-optimization of the system is developed. The technique is based on the co-optimization of the sensor and the read-out circuitry.

The optimization includes two different phases. The first phase is the nominal optimization of the MEMS accelerometer while the second one is the yield-aware optimization which the robustness of the pre-optimized solutions are improved. Regardless of the optimization phase, at the begining of any iteration in the optimization loop, the sensor performance is evaluated using highly accurate analytical models in order to obtain the sensor performances. The sensor used is a capacitive MEMS sensor where the changes at the capacitance values generate the electrical signals to read-out the acceleration level. The capacitance values of the sensor are also evaluated using the analytical models and these capacitances create the capacitive interface circuit of the MEMS sensor. This capacitive interface circuit is integrated into the netlist of the read-out circuitry, together with the feedback components used in the read-out circuitry, in order to generate a system netlist. After that, system level electrical simulations are performed in order to get the MEMS performance such as the measurement range, system noise, total system cost, phase shift delta (phase difference of the system output from 90º) and the power consumption. This performance evaluation flow is shown in Figure 1.

As shown in Figure 2, at the beginning of the optimization, the algorithm runs for several iterations without including the yield concept, in order to create nominally optimized solutions before enhancing the yield. Once the nominal optimization is finished, all objectives are multiplied by a factor which we call the "transition coefficient". For the optimization, an evolutionary optimization algorithm, namely MOEA/D [11] is used. The MOEA/D algorithm replaces existing solutions by newly generated ones only in case there is an improvement in the performance objectives. By using the "transition coefficient" technique in our methodology, the replacement of solutions, which have slightly worse performance than the existing ones but with improved robustness, is promoted. After the update of the objective values using the transition coefficients, one of the yield-aware optimization methodologies reported below are run for several iterations to generate yield-aware PFs.

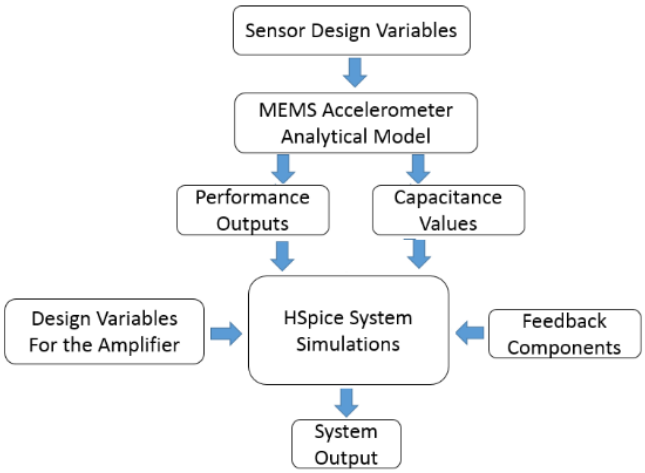

Figure 1. Evaluation flow used for MEMS accelerometer system synthesis [9]

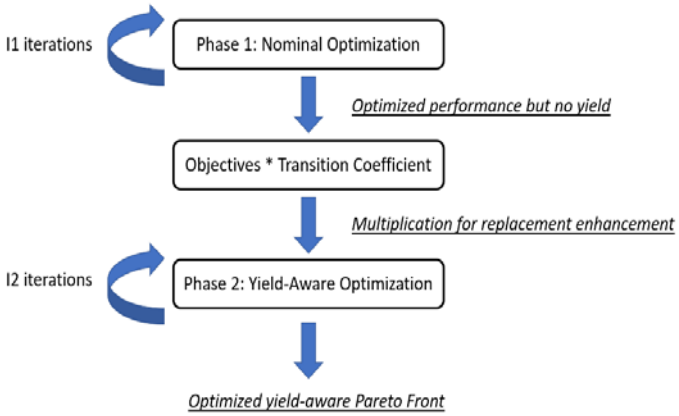

Figure 2. Two-step yield-aware optimization methodology implemented

A dynamic stopping criterion for the nominal optimization, which is based on the hypervolume technique known as Lebesgue measure [12], has been used. In order to empirically determine the optimal transition coefficients, a statistical study based on the trade-off between the optimization efficiency and the replacement probability of the robust solutions has been carried out.

A. *Capacitive MEMS accelerometer system to be optimized*

The capacitive MEMS accelerometer is a combination of the MEMS sensor and the read-out circuitry. The MEMS sensor topology has one moving electrode and two fixed electrodes where two different gaps at the top and bottom sides create a differential capacitance pair with respect to the acceleration direction. These capacitance changes create a voltage signal [9]. The device topology for the MEMS capacitive accelerometer sensor is given in Figure 3.

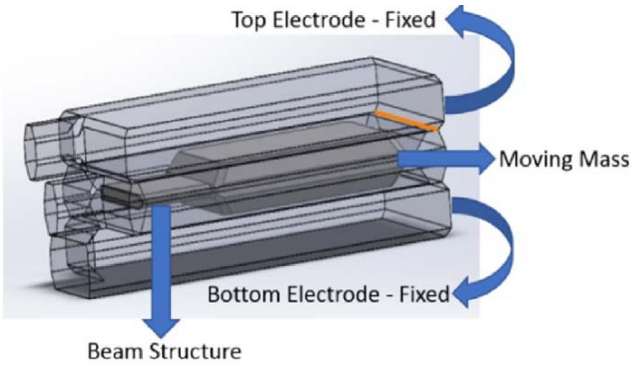

Figure 3. The MEMS capacitive accelerometer sensor

One single MEMS sensor simulation with the MEMS module of the Comsol software [13] takes around 10 minutes. Therefore, running MEMS device simulations in an iterative loop is not an efficient solution for a system-level optimization loop. In a typical evolutionary optimization which is run with a population size *N* along *G* iterations, the number of device simulations needed will be *N.G,* which does not lead to a practical overall simulation time. Moreover, considering yield estimation with MC-based simulations, the use of fast, yet accurate analytical models is enforced [9, 14-16].

For the sensor topology used, highly accurate analytical models have been defined in [9] where the average model error is only 1.3%. The sensor performance is evaluated using these highly accurate analytical models in order to obtain the sensor performances, as well as the capacitance values of the sensor, at the begining of each iteration of the optimization loop. These capacitance values create the capacitive interface of the MEMS sensor and this capacitive interface circuit is integrated into the netlist of the read-out circuitry, to generate a system netlist which is evaluated using electrical simulations.

Figure 4 shows the equivalent electrical circuit of the sensor which is used as a sensor interface for circuit-level simulations. The sensor equivalent circuit consists of two capacitances that are calculated via the sensor analytical model, as well as the sensor noise at the circuit's input node.

A conventional transimpedance amplifier (TIA)-based capacitance-to-voltage (C/V) topology, with a resistance and capacitance feedback has been selected for the analog read-out circuitry. In Figure 5, the system design with the MEMS sensor and the amplifier is given. Any change at the capacitance of the MEMS sensor creates a current which is converted into a voltage value at the output of the amplifier.

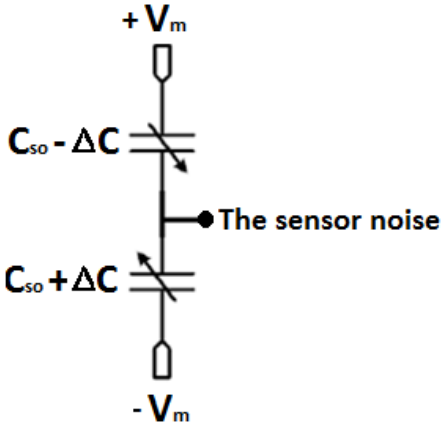

Figure 4. The equivalent circuit used for the MEMS accelerometer sensor [9]

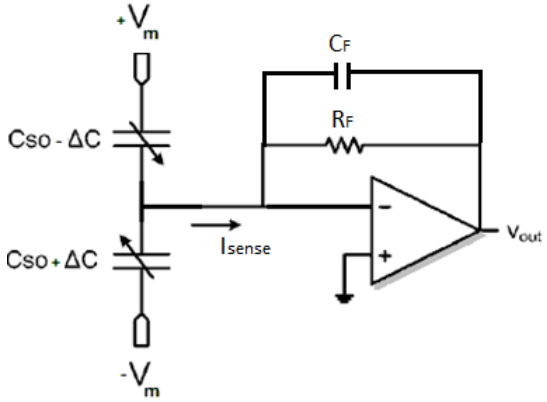

Figure 5. MEMS accelerometer with the TIA-based C/V converter [9]

B. *Co-optimization approach for the accelerometer system*

The co-optimization of the MEMS sensor and the read-out circuitry is performed such that, the sensor performance is evaluated at each iteration of the optimization loop initially, and, then, the capacitive interface generated is used for system level electrical simulations of the MEMS accelerometer system. After the optimization, a yield-aware PF of the MEMS accelerometer is

generated so that the user can select any design point from the PF, which is guaranteed to have a high yield.

The co-optimization technique implemented requires evaluations at both, the circuit and the sensor level. Sensor performance is evaluated using the accurate analytical models while circuit level simulations are performed for the interface and the read-out circuitry. The evaluation flow of the methodology was illustrated in Figure 1.

As shown in Figure 1, in a single iteration, the sensor design variables are initially used to evaluate the sensor analytical model. The performance outputs such as noise and area are extracted from these evaluations, as well as the capacitance values which are used to obtain the capacitive interface of the MEMS sensor. This interface circuit is integrated into the netlist of the read-out circuitry in order to simulate the system level performance outputs, in the same optimization loop. The design variables used during the electrical simulations are introduced at this level as well. After the evaluation of the system level performance values, the optimization algorithm uses these outputs together with the design variables providing these performances, in order to improve the system performance in the following iteration. Figure 6 shows the flow diagram of a single iteration of the implemented optimization methodology for the mixed-domain MEMS accelerometer.

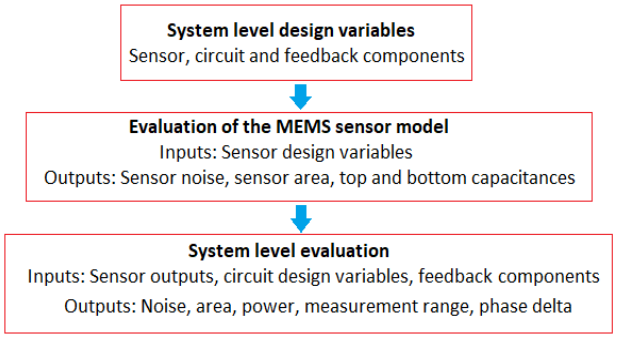

Figure 6. Evaluation of a single iteration in MEMS accelerometer synthesis using the proposed methodology

The system level outputs, i.e., the measurement range, system noise, total system cost, phase delta, and the power consumption, are obtained from the circuit level simulations. These system level performances can be used as objectives or constraints.

C. Yield estimation techniques and selection of QMC-based methodology

Several methodologies are used to embed the variation effects into the optimization loop by realizing the statistical analysis of the system performance. The common ones are MC simulations, MC with some efficiency enhancements, sensitivity-based techniques and design of experiment (DOE) based methodologies.

Due to high accuracy in yield estimation, MC simulations have become the standard technique for statistical analysis and the yield estimation of the integrated circuits. Typically, pseudorandom number generators are used to generate the MC sample sequences. Even though it is highly accurate, a typical yield estimation using MC may involve thousands of electrical simulations, decreasing the efficiency drastically. The most popular strategy to overcome this problem is to improve the sample generator mechanism. Low-discrepancy sequences (LDS) are known as a high performance class of sampling. These sequences are deterministic and have no random component. The points in the sequence are generated to satisfy a uniform coverage among the sampling space. MC simulations which are using these deterministic sequences instead of the pseudorandom sequences are called Quasi-Monte Carlo (QMC) [17]. In this work, a QMC-based methodology has been implemented to accurately estimate the yield of the mixed-domain MEMS. More details on the sample size selection of QMC is given in Section 3. The deterministic sequence used is a Sobol set sequence [18]. The Sobol set is used for the initialization of the QMC samples of all different parameters (both sensor and circuit) with variability information included.

D. CW and IBY techniques

The goal of this paper is synthesizing robust PFs where the yield of each design point on the front is optimized. In order to enhance the yield, the performance variations of the design points need to be improved. The methodology implemented in the paper focuses on decreasing the width of the variation space of the solutions on the final PF. In this paper, two different techniques have been implemented and compared. The illustration of these two different techniques using the variation space of a single solution is given in Figure 7. The single black star in the figure represents the performances of a given solution for nominal technology process parameters; while the blue circles represent the performances of the same solution for a number of samples of the technological process variations. The cloud width (CW) technique is based on the calculation of the Euclidean distances of the performances for all variation samples from the nominal point and finding the maximum distance among all samples for the two limit cases. The IBY (individual-based yield) on the other hand, is based on defining an acceptance region for the nominal solutions by allowing a certain amount of performance variation. The yield is calculated by checking the percentage of the variation samples covered by this acceptance region. The solution is penalized if the pre-defined yield constraint is not satisfied. Both techniques have been implemented as constraints in the optimization loop.

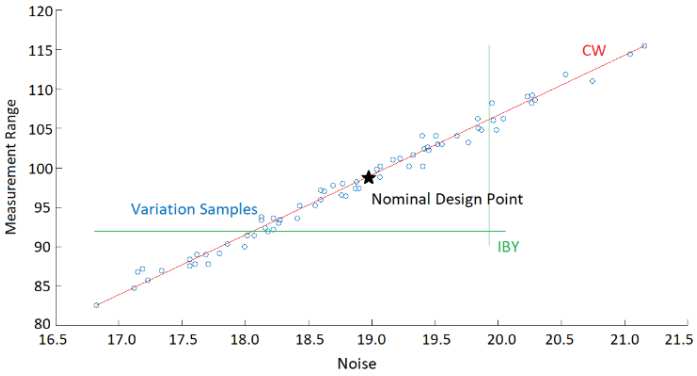

Figure 7. Demonstration of the two yield-aware optimization techniques

In the two-dimensional front given in Figure 7, the CW is shown as the total distance between the lower left corner solution and the nominal solution and the distance between the upper right corner and the nominal solution.

If N is the number of variation samples for each solution point, j is the index for the related sample point, p is the population size, i is the index for the design point on the PF, m is the number of objectives and finally k is the index for the objective, the CW of each single solution point on the PF is calculated as:

For all $1 \leq i \leq p$

$$x_{lim1,i} = \max_{1 \leq j \leq N} \left\{ \sqrt{\sum_{k=1}^{m} \left(x_{i,j} - x_i^{nom}\right)^2} \right\}, \text{ if } \left(x_{i,j} - x_i^{nom}\right) > 0 \quad (1)$$

$$x_{lim2,i} = \max_{1 \leq j \leq N} \left\{ \sqrt{\sum_{k=1}^{m} \left(x_{i,j} - x_i^{nom}\right)^2} \right\}, \text{ if } \left(x_{i,j} - x_i^{nom}\right) < 0 \quad (2)$$

$$CW_i = x_{lim1,i} + x_{lim2,i} \quad (3)$$

To avoid the dominance of any objective value in the Euclidean distance calculation, CW is calculated by using the normalized performance values, with respect to the nominal solution points. Hence, rather than the actual values of objectives, which can be very different from each other, the variation percentages of each single objective will determine the calculated Euclidean distances.

The IBY technique is based on defining an acceptance region for the nominal solutions by allowing a certain amount of performance variation. The yield value for each design point on the PF is calculated by checking the percentage of the variation samples covered by this acceptance region and penalize the solution by adding an extremely high value (considering the optimization has been formulated as minimization problem) if the pre-defined yield constraint is not satisfied.

If p is the population size, i is the index for the design point on the PF, m is the number of objectives, k is the index for the objective, d_k is the user-input for variation percentage allowed for the k^{th} objective, N is the number of variation samples for each solution point, and finally j is the index for the related sample point, the yield value for each design point on the PF is calculated as:

For all $1 \leq i \leq p$ of each $1 \leq j \leq N$, for all maximization objectives:

$$Y_{i,j} = \begin{cases} 1, if\ x_{k,i,j} < (1 - d_k) * x_{k,i}^{nom} \\ 0, otherwise \end{cases} \quad (4)$$

For all minimization objectives:

$$Y_{i,j} = \begin{cases} 1, if\ x_{k,i,j} < (1 + d_k) * x_{k,i}^{nom} \\ 0, otherwise \end{cases} \quad (5)$$

And the yield for each solution is calculated as:

$$Y_i = \frac{\sum_{j=1}^{N} Y_{i,j}}{N} \quad (6)$$

E. The optimization flow

A more detailed description of the robust multi-objective optimization of the MEMS accelerometer system is as follows. First, a nominal optimization is run for a number of iterations, which is determined by the stopping criterion given in Section 3, and this nominal optimization allows the solutions on the PF to be improved until a certain point and also makes sure the solutions are not stalled in order to allow replacement of improved solutions during the yield-aware optimization phase. In order to implement that, a dynamic stopping criterion based on a hypervolume technique called Lebesgue measure [12] has been developed. The applied technique stops the nominal optimization once the increase (improvement) of the Lebesgue Measure (LM) value at a certain iteration is not higher than a certain value. At the end of the nominal optimization phase, all objectives are multiplied by a certain factor, named the transition coefficient, in order to increase the replacement probability when performance variations are introduced.

As pointed out above, the replacement can only take place when both improvement on the nominal solution (due to the working mechanisms of MOEA/D) and the improvement on the robustness of that solution (due to the CW and IBY constraints defined) are satisfied together. The transition coefficient, just like the stopping criterion for the nominal optimization, has been empirically determined. It should be noted that the selection of the transition coefficient creates a trade-off between the convergence speed of the algorithm and the quality of the final PF. If the

number is set too low, the replacements will occur quickly; however, the quality of the solutions might be poor. On the other hand, setting this number too high decreases the probability of the replacements and slows down the entire optimization process, even though the replaced solutions have good quality. That occurs due to the working principle of MOEA/D, which replaces a solution only if there is an improvement. In order to empirically determine the optimal transition coefficient as well as the stopping criterion for the nominal optimization, several statistical checks based on these two parameters have also been studied.

After the nominal optimization, CW or IBY based yield-aware optimization phase takes place. Once a solution is improved and it also has a good robustness (e.g., a satisfied CW constraint), it is replaced by the solution from the previous generation. MOEA/D runs for several iterations to generate improved solutions satisfying the yield-aware constraints, in order to obtain a PF with robust MEMS accelerometer design points.

III. SELECTION OF THE OPTIMIZATION PARAMETERS, DESIGN VARIABLES AND OBJECTIVES

Several parameters for implementing the robust optimization of the MEMS accelerometer system need to be set. As mentioned in Section 2, there are several trade-offs involved in selecting these parameters. In the selection of the number of iterations for nominal optimization and the transition coefficient, the probability of the replacement of a solution with a robust one is the most important factor. Once this probability is high, during the yield-aware optimization phase, the algorithm allows the replacement of the design points which have both improved performance values and which satisfy the yield criterion. This results in a robust, diverse, and optimal PF approximation. The efficiency of the optimization needs to be considered as well.

A. Statistical study for the replacement mechanism enhancement

In order to determine the optimization parameters, 20 different iteration counts and transition coefficient sets have been used to realize a two-dimensional robust optimization of the MEMS accelerometer. The population size for the optimization runs is set to 100 and the number of QMC samples is set to 50, which are two practical values whose selections are explained in more detail in the rest of the paper. The number of iterations for the yield-aware optimization phase was set to a fixed value: 25, in order to eliminate the impact of a varying parameter on the statistical analysis experiments to determine the optimal transition coefficient. The results are shown in Table 1.

Table 1. Statistical checks for optimization parameter determination

Nominal Opt. iteration #	Yield Opt. iteration #	Transition Coef.	Opt. Time (hours)	# Robust Solutions Synthesized	Lebesgue Measure *10^5
0	100	*NA*	21.33	82	2.019
50	50	0.92/1.08	11.25	88	2.098
75	50	0.92/1.08	11.29	89	2.124
95	25	0.92/1.08	5.33	96	2.167
105	25	0.92/1.08	5.35	97	2.192
115	25	0.92/1.08	5.36	54	2.193
125	25	0.92/1.08	5.36	18	2.181
95	25	0.94/1.06	5.32	97	2.18
105	25	0.94/1.06	5.34	98	2.196
115	25	0.94/1.06	5.37	41	2.195
125	25	0.94/1.06	5.39	12	2.187
95	25	0.96/1.04	5.33	98	2.189
105	**25**	0.96/1.04	**5.36**	**96**	**2.215**
115	25	0.96/1.04	5.36	28	2.204
125	25	0.96/1.04	5.4	2	2.194
95	25	0.98/1.02	5.33	60	2.184
105	25	0.98/1.02	5.34	54	2.187
115	25	0.98/1.02	5.36	2	2.193
125	25	0.98/1.02	5.38	0	NA
95	25	1.0/1.0	5.31	38	2.188

The LM for 1000 iterations (able to emulate infinite number of iterations considering no solution replacement, hence improvement, occured after the iteration 265 till 1000) has also been checked in order to identify how much the final PFs have converged to global optimum. This value is obtained for nominal optimization only by averaging three different runs and is equal to $2.221 \,.\, 10^5$. It should be noted the closer any LM value gets to this value, the better the solutions. The transition coefficients are given as pairs. Considering the 0.94/1.06 pair for instance; the objectives to be minimized are multiplied by 1.06 and the objectives to be maximized are multiplied by 0.94.

B. Determination of the stopping criterion for nominal and yield-aware optimizations

It can be seen in Table 1 that if the number of iterations for nominal optimization is set too low, the replacement of the solutions during the robust optimization can be easily realized; however, the quality of the solutions are really low, as suggested by the LM values. On the other hand, setting this number too high decreases the probability of the replacements by so-called "freezing" the design points. Hence, the number of the iterations for the nominal optimization needs to be selected carefully. The experiments for two-dimensional optimization show that, 105 iterations is a good number for the nominal optimization phase, regardless of the selection of the transition coefficient. In order to adapt a dynamic stopping criterion and define a methodology based on these experimental checks, the Lebesgue Measure has been calculated at each single iteration for both two- and three-dimensional optimizations. The stopping criterion applied is based on comparing the Lebesgue Measure at a certain iteration with the

average of the past 20 iterations. If the improvement is less than 0.15%, it is considered that the improvements in the LM are marginal and running further iterations will lower the probability of robust solution replacement in the yield-aware optimization phase.

Three different runs of both two- and three-dimensional optimization has been realized according to the termination criterion based on the LM. For two-dimensional optimization, the nominal optimization has been terminated at iterations 104, 105, and 108, respectively, fitting perfectly with the empirically determined 105 value in Table 1. For three-dimensional optimization, the nominal optimization has stopped at iterations 294, 288, and 289. The LM values obtained at each iteration are given in Figure 8 and Figure 9 for two- and three-dimensional optimizations, respectively. The iteration at which the stopping criterion was satisfied is also shown in the figures.

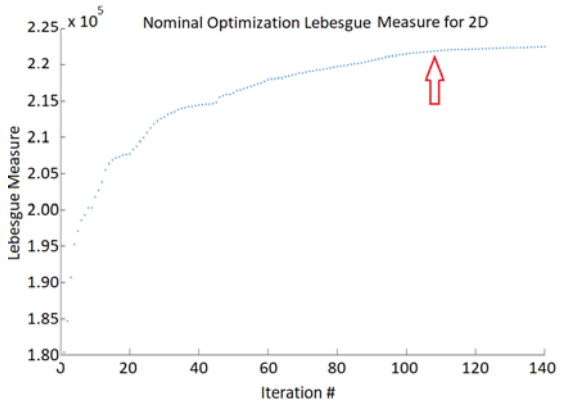

Figure 8. LM through the iterations for two-dimensional optimization

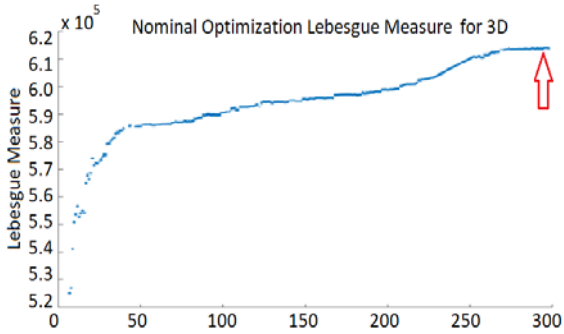

Figure 9. LM through the iterations for three-dimensional optimization

The yield-aware optimization phase runs until two stopping criteria are satisfied. The first one considers the number of solutions in the Pareto Front that are replaced by robust ones. As discussed in Section 2, after the nominal optimization, the yield-aware optimization starts, where the yield-aware Pareto Front is generated by replacing the non-robust solutions with the robust ones. Typically, after 20 to 22 iterations (slightly varying for different methodologies and also different runs of the same methodology), the number of solutions on the robust Pareto Front can achieve 95% of the initially set population sizes, meaning the majority of the solutions have been replaced with robust ones. This percentage has been set as the first stopping criterion.

The second stopping criterion is based on the improvement of the nominal design points. The transition coefficient technique increases the probability of the replacement of the solutions by robust ones; on the other hand, it also allows the replacement of solutions with slightly worse performance. During the yield-aware optimization, the Pareto Front not only improves in terms of the number of robust solutions, but also keeps improving the nominal performances. The LM metric is evaluated after each iteration to check if the starting point value (LM obtained after the last iteration of the nominal optimization) has been reached. Typically, between 23 and 26 yield-aware iterations, this second stopping criterion is also met. Once both criteria are satisfied, the yield-aware optimization phase is stopped to output the final yield-aware PF.

C. Determination of the transition coefficient

Once the nominal optimization is finished, all objectives are multiplied by the transition coefficient in order to increase the replacement probability of the robust solutions during the yield-aware optimization. As described in Section 2, if the transition coefficient number is set too close to 1, which means keeping the original objective values, the probability of replacement will be too low. On the other hand, if the transition coefficient is much smaller than 1, the probability of replacement will drastically increase; however, the quality of the solutions will not be good. Hence, a very high number of iterations at the yield-aware optimization phase will be needed to obtain an optimal PF. As Table 1 suggests, after applying the stopping criterion which correspond to 105 nominal iterations, the selection of the transition coefficients as 0.96/1.04 is the optimal case. Using these values, not only 96 different robust solutions on the PF could be achieved (thanks to high replacement probability), but also a quite high LM ($2.215 \, . \, 10^5$).

D. QMC sample size selection

The selection of the QMC sample size determines the accuracy of the yield estimation. Very low sample sizes will not be able to capture enough variation space, causing an inaccurate yield estimation. A very high sample size, on the other hand, will linearly increase the number of simulations; hence, the overall optimization time will not be practical anymore. An ideal way of selecting the QMC sample size is decreasing the sample size as much as possible, but also guaranteeing that the sampling leads to

a good approximation of the probability distribution function. For that purpose, several QMC sample sizes have been compared by checking the variability information reflected on the different objectives. A probability plot technique called quantile-quantile plot, also known as QQ-Plot, which is a graphical method for comparing two probability distributions by plotting their quantiles against each other, has been used [19].

One example for the QQ-Plot for different QMC sample sizes has been given in Figure 10, which shows the variability behavior of the total measurement range of the MEMS accelerometer system. The x axis is showing the standard normal quantiles, known as sigma or standard deviation in normal distribution, while the y axis is the original simulated values for one design point with process variations. The red line shows the quantiles of an ideal normal distribution function.

QQ-Plots have been obtained for QMC sample sizes of 25, 35, 50, 75, 100 and 1000. An acceptable QMC sample size means a good coverage of the variation space; hence, an accurate yield estimation for the related objective values. As it can be seen from Figure 10, decreasing the QMC sample size to below 35 decreases the variation space covered drastically. Increasing the QMC sample size also increases the variation space covered; however, a very large sample size will require very high number of electrical simulations worsening the efficiency of the optimization drastically. The overall robust optimization time required for a two-dimensional, 100 population size Pareto Front is 5 hours 22 minutes for a QMC sample size of 50. Increasing the QMC sample size to 100 increases the overall robust optimization time to 9 hours 55 minutes with only a marginal improvement in the yield estimation, as the variation spaces shown in the Figure 10 are very similar. A QMC sample size of 1000 on the other hand, will enhance the accuracy of the yield estimation however, an estimated robust optimization time is slightly above 4 days, making it not a practical solution. It should be noted that the optimizations are run on a 1.9 GHz i3-3227 microprocessor.

In order to have a reasonable accuracy for yield estimation and also practical optimization times to obtain yield-aware Pareto Fronts, QMC sample size has been selected as 50 for two-dimensional optimization. For three-dimensional optimization, on the other hand, a technique based on a linear increment of the QMC sample size has been applied at the yield-aware optimization iterations. Using this method, the QMC sample size per solution starts with 46 and goes up to 70 at the last iteration, with a linear increment of one sample per generation. With this methodology, replacements of the robust solutions are realized at the first iterations while the last iterations with higher QMC sample size guarantee the accuracy of the yield estimation. This methodology has been proposed as a generic technique and implemented on three-dimensional yield-aware optimization of the MEMS accelerometer system.

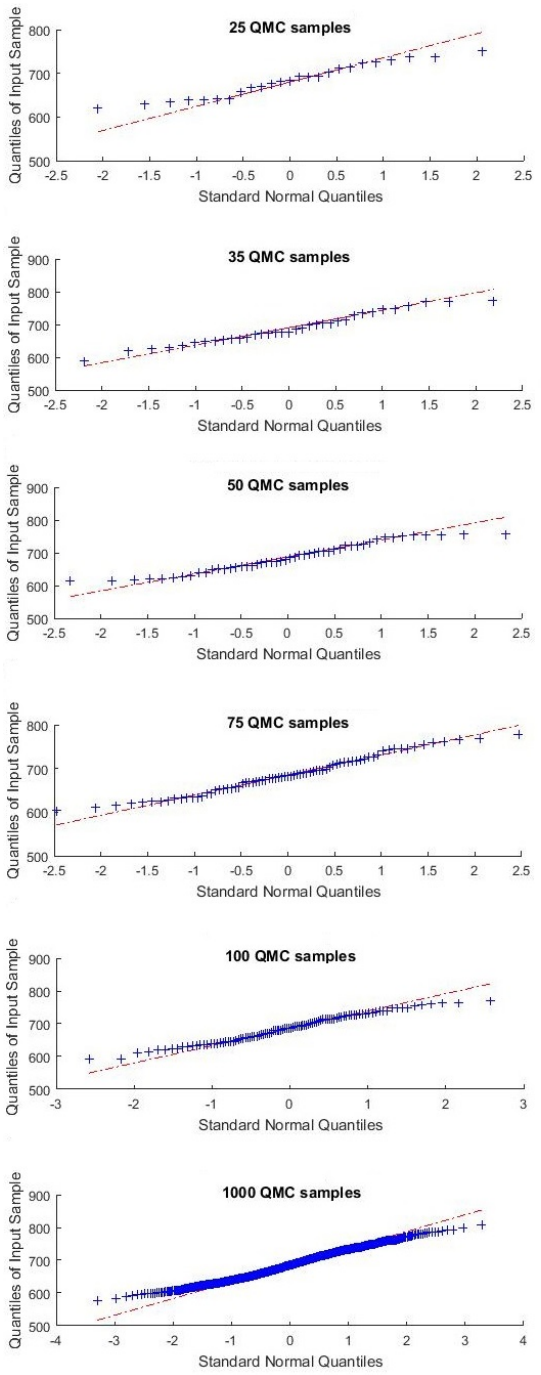

Figure 10. QQ-Plots obtained by different QMC sample sizes for the "measurement range" objective of the MEMS accelerometer system

E. Selection of the yield optimization constraints for CW and IBY

The CW defined in Section 2 is applied as a constraint to penalize the design points in case the CW calculated is above a

certain value, in order to guarantee the survival of robust solutions only, during the yield-aware optimization iterations. For two-dimensional optimization, the CW constraint has been selected as 0.2 (meaning 20% two-dimensional normalized total distance) and 0.27 (meaning 27% three-dimensional normalized distance) for three-dimensional robust optimization of the MEMS accelerometer system. The main motivation for the selection of these values is the initial variability information of the design points obtained after nominal optimization. The average CW for the all design points on the PF has been calculated as around 0.3 for two-dimensional optimization and around 0.4 for the three-dimensional optimization. Setting up the above constraint values, the variability of the solutions generated after yield-aware optimization is guaranteed to have an improvement of above 30%, compared to the results of the nominal optimization.

For the selection of the IBY on the other hand, a practical value of 90% yield has been used as the constraint to decide whether a penalization will be applied to the solutions (by increasing the fitness values of the minimization problem) on the Pareto front or not. The acceptance region is defined by allowing 5% variation (higher or lower depending on the type of the objective) on the nominal solution. With the same motivation as the selection of CW constraint, the selection of these values is based on the initial variability information of the design points obtained after nominal optimization. The average yield for the all design points on the PF has been calculated as around 65% for two-dimensional optimization and around 66% for the three-dimensional optimization. Setting up the above yield constraint to each single solution on the PF, the yield of all the solutions generated after yield-aware optimization is guaranteed to be above 90% for the acceptance region defined.

More details on the CW and yield values obtained after nominal optimization, as well as the robustness improvements obtained, are given in Section 4.

F. Design variables and objectives

The optimization loop includes 20 different design variables. Seven of them (beam and mass thickness, width and length values, as well as the capacitive gap) correspond to the MEMS sensor. These 7 design variables are used in order to obtain the performances such as noise and area using an analytical model, as well as the capacitance values which are used to generate the capacitive interface of the MEMS sensor. This interface circuit is integrated into the netlist of the read-out circuitry in order to simulate the system level performances, in the same optimization loop. The 13 electrical design variables are the bias current, the feedback capacitance, the feedback resistance, transistor width and length values. Using these 13 design variables and the capacitive interface generated by the sensor evaluations, the system level performance is evaluated. Table 2 shows the system design variables and their allowable ranges.

Table 2. Design variables and their allowable ranges

Design Variable	Minimum Value	Maximum Value
$L_{mass}, W_{mass}, W_{beam}$	200 µm	3 mm
t_{mass}	250 µm	500 µm
L_{beam}	200 µm	2 mm
t_{beam}	50 µm	150 µm
C_{gap}	0.5 µm	1.5 µm
$W_{transistors}$	0.5 µm	300 µm
$L_{transistors}$	0.35 µm	30 µm
R_F	10 kΩ	1 MΩ
C_F	0.1 pF	10 pF
I_{bias}	0.5 µA	2.5 mA

There are 13 different transistors in the amplifier. 5 different W and 5 different L values have been defined as design variables since the transistors are in general working as pairs with the same geometry to create the current mirrors. All the 13 transistors use a certain factor of W and L values that are optimized as design variables. The amplifier topology used is given in Figure 11. The optimization for both nominal and yield-aware phase is realized by using these 20 design variables.

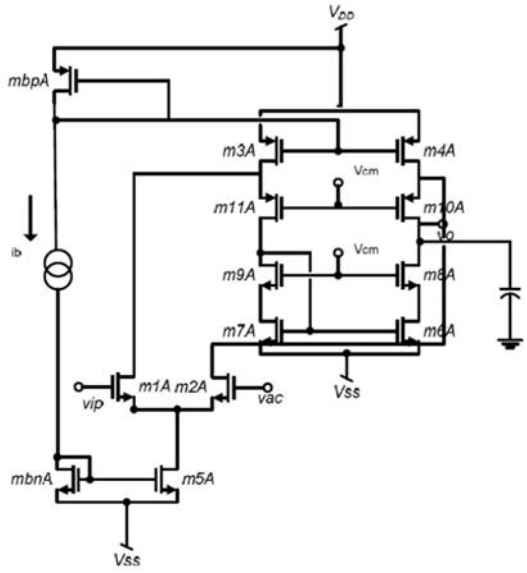

Figure 11. The folded cascode amplifier topology used [20]

In order to embed the variation information for the MEMS sensor, 3-sigma process variation data from the Tubitak Turkey cleanroom facilities has been used. The process variations considered for the length and width of the mass and beam

structures are the geometrical variations which take both lithography and etch variations into account. For the thickness of the mass and the beam structures, the variations of the deep Silicon etch process has been used. The variations on the capacitive gap are defined by the deposition variations of the sacrificial oxide layer which is later removed in order to complete the formation of the capacitive gaps between the electrodes. The variation modeling for MEMS is done by directly adding these fluctuations to the design variables, according to the Tubitak cleanroom process characterization data.

For the electrical simulations, BSIM3v3 models for a 0.35 µm CMOS technology were used. The process variation library for this 0.35 µm technology, which includes several statistical parameters for Monte Carlo simulations, has also been used in the optimization loop, to evaluate the variabilities in the system performance.

Several MEMS accelerometer system performances are obtained after the electrical simulations. They are the overall system manufacturing cost, total system noise, phase shift delta, measurement range and the power consumption.

Phase shift delta is defined as the phase difference of the system output from 90º. The phase shift delta at the output of the C/V converter circuit is an important quality parameter for the MEMS device since the output signal is likely to be modulated.

The total system cost, on the other hand, is calculated in USD, with the assumption of a hybrid manufacturing approach in which the sensor and the circuit including the feedback components are manufactured seperately and, then, bonded. The manufacturing cost is 58 $cents/mm^2$ for the CMOS read-out circuitry and 16 $cents/mm^2$ for the sensor. These cost values were obtained from the cleanroom facility of Tubitak Turkey and they are the cost per area standard for the standard CMOS and MEMS manufacturing. With the additional two US dollars, which correspond to the packaging cost, the total cost of the overall system can be calculated as:

$$total_{cost} = 0.58 * Area_{electronics} + 0.16 * Area_{sensor} + 2 \quad (7)$$

In two-dimensional robust optimization, the total system noise and the measurement range has been selected as the objectives which the yield-aware PFs are synthesized for. For three-dimensional robust optimization, phase shift delta has been added as the third objective while all other specifications are defined as system constraints. Table 3 shows the system level specifications for two-dimensional robust optimization while Table 4 shows the system level specifications for three-dimensional robust optimization of the MEMS accelerometer system.

Table 3. System level specifications for two-dimensional optimization

Performance - System	Value
Total System Noise ($\mu g/\sqrt{Hz}$)	Minimize (Objective 1)
Measurement Range (g)	Minimize (Objective 2)
Phase Shift Delta (º)	< 3
Power Consumption (µW)	< 500
System Manufacturing Cost (USD)	< 5

Table 4. System level specifications for three-dimensional optimization

Performance - System	Value
Total System Noise ($\mu g/\sqrt{Hz}$)	Minimize (Objective 1)
Measurement Range (g)	Minimize (Objective 2)
Phase Shift Delta (º)	Minimize (Objective 3)
Power Consumption (µW)	< 500
System Manufacturing Cost (USD)	< 5

IV. YIELD-AWARE OPTIMIZATION RESULTS

In order to demonstrate the proposed methodology, two- and three-dimensional yield-aware optimizations have been run.

A. Two-dimensional yield-aware optimization results

Two-dimensional robust optimization of the MEMS accelerometer system has been run using a population size of 100. Initially, the nominal optimization is run until the LM based stopping criterion is satisfied. This is based on calculating the LM value at each iteration and checking if the improvement compared to the average of past 20 iterations is below 0.15%. After the nominal optimization phase, the transition coefficients are applied and yield-aware iterations including the variability information of the CMOS, passive devices and the MEMS sensor are run until the two stopping critera defined in Section III-B are reached, in order to obtain robust MEMS design points on the final PF. Both CW and IBY methodologies have been implemented and compared for yield optimization. The QMC sample size used for the two-dimensional yield-aware optimization is 50. The yield-aware optimization results have also been compared with the results obtained with nominal optimization to show the improvements on the device robustness. For the nominal optimization results (where no yield-aware optimizations are run) which are compared with CW and IBY in Tables 6-9, some extra nominal optimization iterations have been run (which is equal to the number of yield-aware iterations determined by the two different stopping criteria) after the stopping criterion of nominal optimization is satisfied, in order to make the overall number of iterations, hence the number of simulations for the nominal design

points, equal. The overall yield-aware optimization time required has an average of 5 hours 25 minutes using a 1.9 GHz i3-3227 microprocessor. In order to have a fair comparison, 8 different design points obtained using different techniques, which have similar system noise and measurement range values have been identified and the results are shown in Table 5. The Figure-of-Merit for two-dimensional optimization is:

$$FOM_{2D} = Measurement\ Range/Total\ System\ Noise \quad (8)$$

Table 5. Comparison of eight adjacent solutions obtained with different techniques

Design Point #1	**CW**	**IBY**	**Nominal**
Noise	20.17	20.25	20.11
Measurement Range	170.0	169.6	170.1
FOM	8.43	8.38	8.46
Yield	81.88%	90.12%	69.14%
Design Point #2	**CW**	**IBY**	**Nominal**
Noise	29.73	29.82	29.68
Measurement Range	285.8	284.8	285.8
FOM	9.61	9.55	9.63
Yield	83.44%	90.72%	63.12%
Design Point #3	**CW**	**IBY**	**Nominal**
Noise	39.98	40.01	39.94
Measurement Range	407.0	404.9	408.2
FOM	10.18	10.12	10.22
Yield	82.65%	90.81%	66.24%
Design Point #4	**CW**	**IBY**	**Nominal**
Noise	50.54	50.87	50.52
Measurement Range	535.6	534.8	536.9
FOM	10.60	10.51	10.63
Yield	80.77%	90.44%	58.45%
Design Point #5	**CW**	**IBY**	**Nominal**
Noise	60	59.98	59.96
Measurement Range	649.4	643.6	650.6
FOM	10.82	10.73	10.85
Yield	80.61%	91.83%	57.45%
Design Point #6	**CW**	**IBY**	**Nominal**
Noise	70.44	70.55	70.46
Measurement Range	769.2	766.9	772.2
FOM	10.92	10.87	10.96
Yield	80.41%	92.22%	62.71%
Design Point #7	**CW**	**IBY**	**Nominal**
Noise	80.22	80.46	80.11
Measurement Range	886.8	883.7	889.6
FOM	11.05	10.98	11.10
Yield	81.44%	90.20%	66.34%
Design Point #8	**CW**	**IBY**	**Nominal**
Noise	90.45	90.48	90.39
Measurement Range	990.6	985.3	991.6
FOM	10.95	10.89	10.97
Yield	82.65%	94.89%	68.84%

In Table 6, the average yield values and the objective variations (defined as the two-dimensional CW as shown in Figure 7) obtained from all the solutions on the final PF is given. In order to calculate the yield values for each design point, an acceptance region is defined by allowing 5% variation (higher or lower depending on the objective) on the nominal solution. Hence, it should be noted that the yield values reported are based on the acceptance regions defined for each single nominal design point and comprising the robustness (low-variability) information of each single solution.

Table 6. Comparison of the average yield and variation values for all the solutions on the two-dimensional PFs

Performance \ Technique	**CW**	**IBY**	**Nominal**
2D Variation: Cloud Width (CW)	19.71%	17.50%	30.17%
Yield	81.23%	90.55%	65.10%

The results suggest that for both CW and IBY techniques, the nominal design points generated by the yield-aware optimization tool are comparable with the outputs of a nominal optimization but with a much better yield performance. Hence, the robustness of the solutions on the final PF has been drastically improved. Using the CW technique, the yield obtained is improved compared to nominal optimization but it is worse than the yield values obtained by the IBY. The CW has marginally better nominal design points compared to IBY.

B. Three-dimensional yield-aware optimization results

Three-dimensional robust optimization of the MEMS accelerometer system has been run by considering the phase shift delta as the third objective and using a population size of 200. Very high population sizes will require a high number of simulations, increasing the overall run time of the optimization. Especially, considering the yield-aware QMC simulations, the population size should not be kept too high. A small population size, on the other hand, will not be able to capture the entire search space of the solution space; hence, lowering the diversity of the solutions on the final PF.

Identical to the two-dimensional optimization, initially, a nominal optimization is run until the stopping criterion is satisfied. After applying the transition coefficients, yield-aware iterations are run until the two stopping critera are satisfied in order to obtain a three-dimensional PF with robust MEMS design points. CW and IBY methodologies have been both adapted in the optimization loop and compared for yield optimization. The QMC sample size used for the yield-aware optimization starts with 46 and goes up to 70 at the last iteration, with a linear increment of one sample per iteration. The goal is guaranteeing the accuracy of the yield values calculated at the final iterations while the first iterations can realize the replacements of the robust solutions relatively faster. This methodology has been applied to three-dimensional optimization only in order to enable a higher QMC sample size, which is required due to increased number of dimensions, with a reasonable optimization time. The overall yield-aware

optimization time required has an average of 15 hours 20 minutes using a 1.9 GHz i3-3227 microprocessor.

The nominal optimization results have also been used for the yield comparisons. For the nominal optimization results obtained, some extra iterations (equal to the number of yield-aware iterations for robust optimization) have been run after the stopping criterion is satisfied, just like in the two-dimensional PF comparisons.

A direct comparison of 3 different design points per technique, with a very similar system noise, measurement range, and phase shift delta performance has been obtained as given in Table 7.

The Figure-of-Merit for three-dimensional optimization is calculated as:

$$FOM_{3D} = Measurement\ Range/(Total\ System\ Noise * Phase\ Shift\ Delta) \quad (8)$$

The acceptance region for yield calculations is again defined by allowing 5% objective variation based on the nominal design points obtained.

Table 7. Comparison of three adjacent solutions obtained with different techniques

Comparison #1	**CW**	**IBY**	**Nominal**
Noise	18.08	17.77	19.08
Measurement Range	103.40	96.40	97.80
Phase Shift Delta	1.86	1.81	1.62
FOM	3.07	3.00	3.16
Yield	80.00%	91.42%	65.72%
Comparison #2	**CW**	**IBY**	**Nominal**
Noise	58.87	59.33	58.31
Measurement Range	450.60	450.10	457.40
Phase Shift Delta	0.58	0.58	0.59
FOM	13.20	13.08	13.30
Yield	82.85%	90.00%	67.14%
Comparison #3	**CW**	**IBY**	**Nominal**
Noise	91.57	94.32	97.85
Measurement Range	912.40	922.12	903.60
Phase Shift Delta	1.44	1.43	1.32
FOM	6.92	6.84	7.00
Yield	81.42%	91.42%	62.86%

Table 8, on the other hand, shows the average yield values and the variations, defined as CW, obtained from all the solutions on the final PF.

Table 8 Comparison of the average yield and variation values for all solutions on the three-dimensional PFs

Performance \ Technique	**CW**	**IBY**	**Nominal**
3D Variation:			
Cloud Width (CW)			
Yield	80.48%	90.69%	66.65%

The results for three-dimensional robust optimization also suggest that for both CW and IBY techniques, the nominal design points generated by the yield-aware optimization tool are comparable with the outputs of a nominal optimization but with a drastically better yield performance. The robustness of the solutions on the final PF has been improved with both methodologies. The FOMs obtained with the CW technique are marginally better than the ones obtained with the IBY; however, the yield of the solutions are significantly worse. Hence, the same findings observed in two-dimensional optimization is also valid for three-dimensional optimization.

Figures 12, 13, and 14 show the variations on the system performance for the first design points in Table 8 obtained using the CW methodology and the nominal optimization.

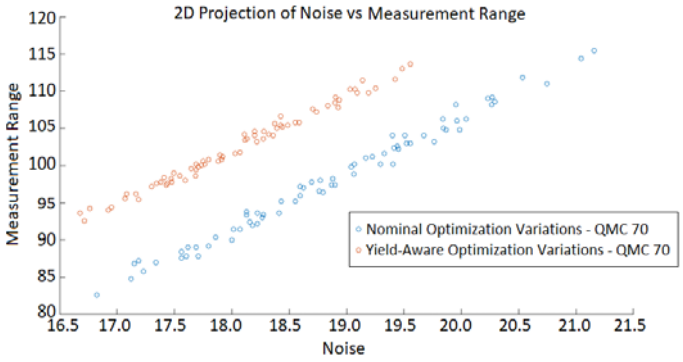

Figure 12. Noise vs Measurement Range performance variation of a single solution for CW vs Nominal Optimization

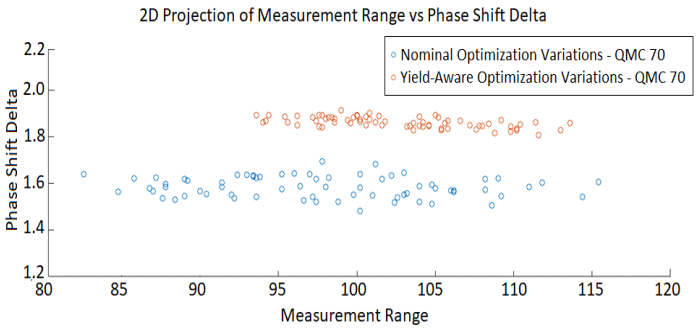

Figure 13. Measurement Range vs Phase Shift Delta performance variation of a single solution for CW vs Nominal Optimization

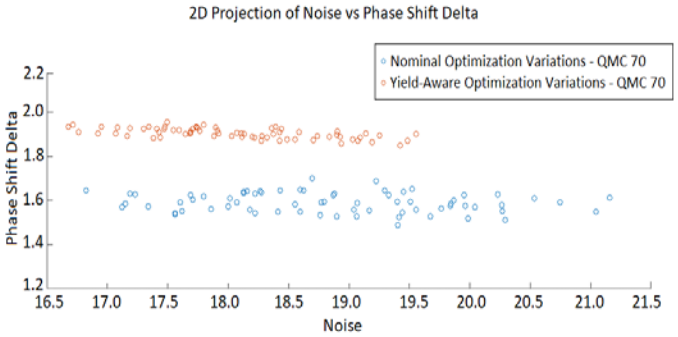

Figure 14. Noise vs Phase Shift Delta performance variation of a single solution for CW vs Nominal Optimization

The QMC sample size is 70 as the results are extracted from the final PF. The variations on the nominal performances are shown as two-dimensional projections of the three objectives.

The results demonstrate the decrease in the variability obtained by using the yield-aware optimization methodology proposed.

In order to guarantee the accuracy of the yield estimation, a 10,000 sample MC simulation has been run for the first design points compared in Table 7. Table 9 shows the yield values obtained using 10,000 sample MC analysis.

Since the QMC is deterministic and has no natural variance, there is no practical way to determine the confidence interval of the estimated yield. This issue has been address in [21] and [22] and a solution has been proposed and implemented by running a scrambled QMC, in which samples are randomly permuted, several times to obtain a stochastic variance. In order to obtain the confidence intervals for the estimated yield, this technique has been used by running 20 different scrambled QMC on the nominal design parameters of each design point. The confidence intervals of the yield estimations with 99% confidence level are also given in Table 9.

The confidence interval for MC (10.000 samples) with 99% confidence level, on the other hand, is calculated based on [23] and included in Table 9.

Table 9. Comparison of the yield obtained using QMC and MC for the first solutions obtained with different techniques

Comparison #1	CW	IBY	Nominal
Noise	18.08	17.77	19.08
Measurement Range	103.40	96.40	97.80
Phase Shift Delta	1.86	1.81	1.62
FOM	3.07	3.00	3.16
Yield: QMC 70 Samples	80.00%	91.42%	65.72%
Yield: MC 10,000 Samples	76.15%	88.72%	61.63%
Confidence Interval (99%) for 70 sample QMC	74.61%≤x ≤80.25%	86.92%≤x≤91.50%	60.61%≤x≤66.07%
Confidence Interval (99%) for 10,000 sample MC	75.06%≤x ≤77.24%	87.91%≤x≤89.53%	60.41%≤x≤62.85%

The results show that the yield calculations based on 70 sample QMC and 10,000 sample MC (which can be considered as exact yield) are quite similar to each other, with around and less than 4% deviation on the yield estimation. Hence, the QMC-based methodology can accurately model the yield for the MEMS accelerometer system optimized. Moreover, all MC simulation results are in the confidence interval calculated.

V. CONCLUSION

The paper is focused on a novel yield-aware optimization methodology which can be used for the multi-objective robust optimization of the mixed-domain systems, such as MEMS. The methodology has been evaluated using a MEMS accelerometer system which includes a capacitive MEMS sensor and an analog read-out circuitry. In the synthesis loop, two different phases of optimization occurs. During the first phase, nominal optimization of the MEMS accelerometer system is performed until the stopping criterion defined. After that, a second phase, where the yield of the solutions on the PF are improved, follows. Two different approaches for the yield optimization have been implemented. A QMC-based methodology has been used to embed the variation effects into the optimization loop. The results for both two- and three-dimensional yield-aware optimization are quite promising for robust MEMS accelerometer sensor-circuit co-design.

REFERENCES

[1] T. Tan, S. Roy, N. Thuy and H. T. Huynh, "Streamlining the Design of MEMS Devices: An Acceleration Sensor", *IEEE Circuits and System Magazine*, pp. 18–27, March 2008.

[2] Y. Zhang, R. Kamalian, A. M. Agogino, C. H. Séquin, "Hierarchical MEMS Synthesis and Optimization", *Proceedings of SPIE, International society for optical engineering*, vol. 5763, May 2005.

[3] R. Neul et al., "A Modeling Approach to Include Mechanical Microsystem Components into the System Simulation", *Proc. Design , Automation and Test in Europe Conf., DATE, February* 1998

[4] M. Pak, F.V. Fernandez, G. Dundar,"Optimization of a MEMS Accelerometer Using MOEA/D Evolutionary Algorithm ", *Proc. Int. Conf. On Synthesis, modeling, analysis and simulation methods and applications to circuit design (SMACD)*, July 2017

[5] Z. Fan et al., " Hierarchical Evolutionary Synthesis of MEMS " , *IEEE Congress on Evolutionary Computation,* pp. 2320-2327, September 2004.

[6] T. Mukherjee, G. Fedder, "Hierarchical Mixed-Domain Circuit Simulation, Synthesis and Extraction Methodology for MEMS", *Journal of VLSI signal processing systems for signal, image and video technology*, vol. 21, issue 3, pp. 233–249, July 1999

[7] C. Zhao, T. J. Kazmierski, " Automated Performance Optimization and Layout Synthesis of MEMS Accelerometer with Sigma-Delta Force - Feedback Control Loop", *Proc. IEEE Behavioral Modeling and Simulation Workshop,* September 2008

[8] J. Klaus, R. Paris, R. Sommer, "Systematic MEMS ASIC Design Flow using the Example of an Acceleration Sensor ", *Proc. Int. Conf. On synthesis, modeling, analysis and simulation methods and applications to circuit design (SMACD),* June 2016

[9] M. Pak, F.V. Fernandez, G. Dundar, " A Novel Design Methodology for the Mixed-Domain Optimization of a MEMS Accelerometer ", *Integration, the VLSI Journal,* pp. 314-321, April 2018

[10] F. Burcea, A. Herrman, B. Li, H. Graeb, " MEMS – IC Optimization Considering Design Parameters and Manufacturing Variation from both Mechanical and Electrical Side " , *25th IEEE International Conference on Electronics, Circuits and Systems (ICECS),* December 2018

[11] Q. Zhang, H. Li, "MOEA/D: A Multiobjective Evolutionary Algorithm based on Decomposition", *IEEE Transactions on Evolutionary Computation*, pp. 712-731, November 2007.

[12] M. Fleischer, " The Measure of Pareto Optima. Applications to Multi-Objective Metaheuristics", *Conference on Evolutionary Multi - Criterion Optimization (EMO 2003)*, Springer, vol. 2632 of LNCS, pp.519-533, April 2003

[13] COMSOL Software , MEMS Module by *Comsol Multiphysics GmbH*, https://www.comsol.com/mems-module. [Accessed September 5th, 2019]

[14] T. Belendez, C. Neipp, A. Belendez, " Large and small deflections of a cantilever beam", *European Journal of Physics,* vol. 23, no. 3, pp.371-379, May 2002

[15] J. Strong et al., "Carbon MEMS Accelerometer", Proceedings of the Comsol Conference, Boston, June 2011

[16] B.E. Boser, R. T. Howe, "Surface Micromachined Accelerometers", *IEEE Custom Integrated Circuits Conference*, pp. 337-344, May 1995

[17] M. Pak, F. V. Fernandez, G. Dundar, " Comparison of QMC-based Yield-aware Pareto Front Techniques for Multi-objective Robust Analog Synthesis " , *Integration , the VLSI Journal* , vol. 55, no. 9, pp.357-365, September 2016

[18] D. Ivan, G. Rayna,"Monte Carlo Method for Numerical Integration Based on Sobol's Sequences", Numerical Methods and Applications, pp.50-59, August 2010

[19] M. B. Wilk, R. Gnanadesikan, "Probability Plotting Methods for the Analysis of Data ", Biometrika, Vol. 55, No. 1, pp. 1-17, March 1968

[20] B. Liu et al, "An Enhanced MOEAD/DE and its Application to multiobjective analog cell sizing", *IEEE Congress on Evolutionary Computation,* pp. 1-7, July 2010

[21] E., Afacan, B. Gonenc, A. E., Pusane, G., Dundar, F., Baskaya, "A Hybrid Quasi Monte-Carlo Method for Yield Aware Analog Circuit Sizing Tool" *Design, Automation and Test in Europe Conference and Exhibition (DATE)*, pp. 1225-1228, 2015

[22] H. Morohosi, M. Fushimi, "A Practical Approach to the Error Estimation of Quasi – Monte Carlo Integration", *Monte Carlo and Quasi - Monte Carlo Methods*, vol. 377, p. 390, 1998.

[23] H., Graeb, "Analog Design Centering and Sizing", Springer, 2007